Detiding Measurement on Transport of the Changjiang-Derived Buoyant Coastal Current

ARTICLE *in* JOURNAL OF PHYSICAL OCEANOGRAPHY · NOVEMBER 2013

Impact Factor: 2.86 · DOI: 10.1175/JPO-D-12-0158.1

8 AUTHORS, INCLUDING:

Hui Wu
East China Normal University
21 PUBLICATIONS **195** CITATIONS

SEE PROFILE

Bing Deng
East China Normal University
25 PUBLICATIONS **347** CITATIONS

SEE PROFILE

Jun Hu
Qingpu District Envrionmental Protection Bureau,Shangh..
9 PUBLICATIONS **54** CITATIONS

SEE PROFILE

Jing Zhang
Fourth Military Medical University
678 PUBLICATIONS **9,381** CITATIONS

SEE PROFILE

Detiding Measurement on Transport of the Changjiang-Derived Buoyant Coastal Current

HUI WU, BING DENG, RUI YUAN, JUN HU, JINGHUA GU, FANG SHEN, JIANRONG ZHU, AND JING ZHANG

State Key Laboratory of Estuarine and Coastal Research, East China Normal University, Shanghai, China

(Manuscript received 19 August 2012, in final form 22 May 2013)

ABSTRACT

Measuring the transport of the Changjiang (also known as the Yangtze) River–derived buoyant coastal current, that is, the Min–Zhe Coastal Current, is of great importance for understanding the fate of terrestrial materials from this large river into the open ocean, but it is usually difficult to achieve because of the energetic tidal currents along the Chinese coast. In February 2012, a detiding cruise survey was carried out using the phase-averaging method. For the first time, this coastal current has been quantified with in situ data and has been shown to have a volume transport of 0.215 Sv (1 Sv $\equiv 10^6\,m^3\,s^{-1}$) and a maximum surface velocity of $\sim$50 cm s^{-1}. The ratio between the volume transport of the buoyant coastal current and that of the Changjiang is $O(10)$. Freshwater transport by the buoyant coastal current accounts for over 90% of the Changjiang River's discharge. Buoyancy and winds are both important in driving this current.

1. Introduction

Buoyant estuarine waters often propagate downshelf along the coast (Garvine 1995; Simpson 1997; Fong and Geyer 2002; Whitney and Garvine 2005), a phenomenon that has been widely observed around the world (Guan 1978; Howden and Murtugudde 2001; Hickey et al. 2005; Lentz and Largier 2006). These buoyant coastal currents transport terrigenous materials, first onto the inner continental shelves and then into the open ocean, playing a key role in the regional material circulations. Quantifying the volume transport of these currents and their ability in transporting the riverine freshwater (thereby the dissolved materials) are of essential importance. In the past, several studies have provided some theoretical estimations of the volume transport of a buoyant coastal current based on the thermal–wind relationship (Yankovsky and Chapman 1997; Avicola and Huq 2002; Fong and Geyer 2002; Pimenta et al. 2011). As the buoyant coastal currents are modulated by the wind (Münchow and Garvine 1993; Whitney and Garvine 2005; Lentz and Largier 2006), tides (Li and Rong 2012), bathymetry, and other forcings, the real transport may be different from these density-based estimations. Hence, in situ measurements are necessary.

To get a detailed cross-sectional structure, and thereby the transport of a buoyant coastal current, a cruise survey is generally required. However, this is often a difficult task, especially in areas disturbed by energetic tides. Spatially distributed long-term detiding (i.e., removing the tidal signals from the observations) cruise surveys are rarely available, though a successful example has been reported for the Faroe–Shetland Channel and Iceland–Faroe Ridge (Rossby and Flagg 2012). Mooring current meters are more widely used to measure the subtidal speed of the coastal currents (e.g., Geyer et al. 2004; Zeng et al. 2012). Yet, moorings are often too sparse for the transport estimations. In the present study, by a carefully designed special cruise survey, we were successful in obtaining the subtidal cross-sectional profiles of current, salinity, and temperature of the buoyant coastal current from the Changjiang (also known as the Yangtze) River. This current is more widely known as the Min–Zhe Coastal Current (MZCC). From the results, the volume and freshwater transports of the MZCC were quantified for the first time.

The Changjiang is a major source of terrigenous materials for the marginal seas of the northwestern Pacific Ocean. Globally, the freshwater discharged from the continents is estimated to be 1.2 Sv (1 Sv $\equiv 10^6\,m^3\,s^{-1}$) (Dai and Trenberth 2002), of which the Changjiang

Corresponding author address: Hui Wu, State Key Laboratory of Estuarine and Coastal Research, East China Normal University, Shanghai, 200062, China.
E-mail: hwu@sklec.ecnu.edu.cn

DOI: 10.1175/JPO-D-12-0158.1

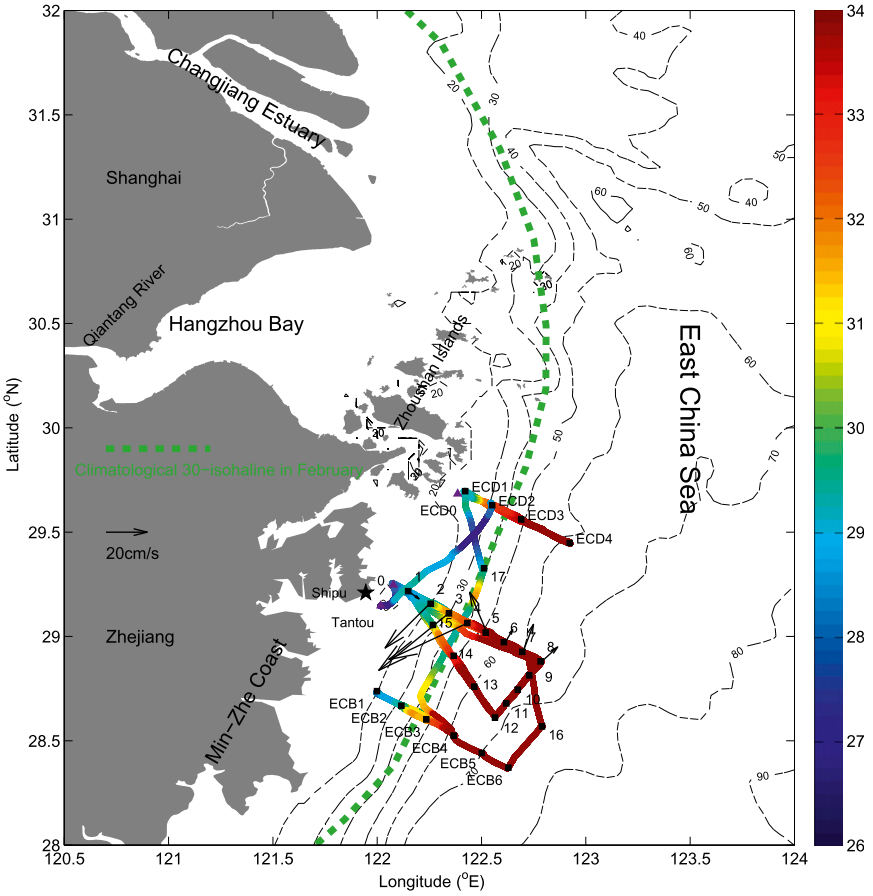

FIG. 1. Survey location and bathymetry around the Min–Zhe Coast area. Rectangular dots signify the sampling sites, and triangular dots represent the anchored sites. The PAM survey was conducted at sites 1–15. The colored line shows the observed surface salinity. Arrows show the observed residual current at 4.25 m below the sea surface. The dashed green line signifies the climatological 30 isohaline in February that is digitized from Editorial Board for Marine Atlas (1992).

accounts for ~2.4% with an annual-mean runoff of ~29 × 10^3 m^3 s^{-1} (Shen et al. 2003). Locally, the Changjiang is responsible for over 90% of the total terrestrial freshwater input into the Yellow and East China Seas. Draining a large basin that is heavily impacted by human activities, the Changjiang transports large amounts of sediments (Deng et al. 2006; Liu et al. 2006), nutrients (Liu and Zhang 2000; Chen 2008), and riverine organic matter (Lin et al. 2002) into the East China Sea. The Changjiang plume propagates downshelf along the Zhejiang and Fujian Coasts (more widely known as the Min–Zhe Coast) in fall, winter, and early spring (Niino and Emery 1961; Guan 1978; Beardsley et al. 1985; Milliman et al. 1985), forming the well-known MZCC, which can be seen from the climatologic 30 isohaline in February (Fig. 1) and several other months (Editorial Board for Marine Atlas 1992). The MZCC transports a great portion of Changjiang-derived materials downshelf along the Min–Zhe Coast, and is characterized by low salinity, low temperature, and high nutrient content (Qiao et al. 2006; Lü et al. 2006). Quantifying the MZCC is essential for understanding the fates of Changjiang-derived sediments and nutrients in the East China Sea.

The Min–Zhe Coast extends a distance of ~500 km. The water depth is less than 20 m near the coast, and increases rapidly offshore to 50–60 m with an almost constant slope (see Fig. 1). This bathymetry was formed by the historic deposition of the Changjiang-derived sediments that were transported by the MZCC (Liu et al. 2006). Tides are significant along the Min–Zhe Coast, with the maximum surface tidal current speed of $O(1)$ m s^{-1} near the coast (unpublished data observed by the State Key Laboratory of Estuarine and Coastal Research). The tide type is regular semidiurnal, and the M_2 constituent is dominant (Su and Yuan 2005). Besides the MZCC, the northward-flowing Taiwan Warm Current (TWC) can sometimes reach the offshore region

(Zhu et al. 2004). In such an energetic environment, quantifying the MZCC is challenging. In a recent modeling study, Li and Rong (2012) estimated that the MZCC transport is 0.12 Sv, and that ~80% of the freshwater from Changjiang is transported by this current, as controlled by a runoff of $10 \times 10^3\,m^3\,s^{-1}$ and tides. Their study revealed the important role of tide in modulating the MZCC. Their model experiments did not consider the wind or the background shelf currents, so it is necessary to know how the MZCC behaves in a realistic environment. Observation is of the first-order importance in oceanography, but in situ data of the MZCC are lacking. As is often the case for buoyant coastal currents, existing observations of the MZCC only cover one or a few sites (Guan 1978; Zhu et al. 2004; Zhang et al. 2011; Zeng et al. 2012), from which the estimation of transport is difficult. Without detailed knowledge of the MZCC, we can only qualitatively understand the influences of the Changjiang on the East China Seas.

To provide a more quantitative understanding, the State Key Laboratory of Estuarine and Coastal Research (SKLEC) at East China Normal University (ECNU) conducted field observations in the region of the Min–Zhe coastal waters (Fig. 1) on 5–14 February 2012. The phase-averaging method (PAM; Katoh et al. 1996, 2000) was used to design and conduct the cruise survey. The remainder of this paper is arranged as follows. Section 2 includes detailed theoretical analyses of PAM, the associated error estimations, and the data sampling processes. Results of the observations are shown in section 3, including the subtidal currents and the salinity/temperature/density profiles across the MZCC. Dynamics of the MZCC are discussed in section 4. Finally, we draw our summary in section 5.

2. Methods

a. The phase-averaging method

As summarized by Chang et al. (2008), there are three basic approaches to remove tidal signals from the acoustic Doppler current profiler (ADCP) data observed by a moving ship: 1) using long-term repeated surveys to construct time series of currents at selected sites, then extracting the tidal current by using harmonic analysis (Simpson et al. 1990; Rossby and Flagg 2012); 2) fitting specific functions, such as polynomial or biharmonic splines, to the ADCP data to determine the spatially varying amplitudes and phases of major tidal constituents (Candela et al. 1992; Münchow 2000); and 3) PAM (Katoh et al. 1996; 2000). PAM removes the tidal signals by repeating the survey with an interval related to the period of the dominant tidal constituent. Although PAM has been used in several oceanographic studies (e.g., Liu et al. 2000; Jan and Chao 2003; Chang et al. 2008), it has not been used to study the buoyant coastal currents. Here, we give theoretical analyses on the rationale of PAM and its error estimations, which have rarely been discussed in previous studies. In a coastal region, the natural current consists of both tidal and subtidal components:

$$V = V_r + \sum_{i=1}^{k} V_i \cos(\omega_i t + \varphi_i), \tag{1}$$

where V_r is the residual current, and V_i, ω_i, and φ_i are the amplitude, angular frequency, and phase lag of each tidal current constituent, respectively. Here we only consider one direction of the current for simplicity, and it is easy to prove that the following approaches are also valid for another current direction. Repeating the survey with rounds M and interval N gives the averaged velocity V_m:

$$V_m = V_r + \frac{1}{M}\sum_{i=1}^{k} V_i \sum_{m=1}^{M} \cos\{\omega_i[t_0 + (m-1)N] + \varphi_i\}, \tag{2}$$

where t_0 is the initial sampling time. For V_m to equal V_r, the second term of the rhs of (2) should be zero. For simplicity, let us first consider a single tidal constituent. After averaging, the residual of this tidal component is

$$\begin{aligned} R_i &= V_i \frac{1}{M}\sum_{m=1}^{M} \cos[\omega_i(m-1)N + \omega_i t_0 + \varphi_i] \\ &\equiv V_i \mathrm{Er}_i, \end{aligned} \tag{3}$$

where Er_i is defined as the relative error. The phase that is determined by the location and initial sampling time is $\omega_i t_0 + \varphi_i$ —for simplicity, we note it as φ. Hence,

$$\begin{aligned} \mathrm{Er}_i = \frac{1}{M}\Bigg\{ &\cos(\varphi)\sum_{m=1}^{M}\cos\left[\frac{2\pi}{T_i}(m-1)N\right] \\ &- \sin(\varphi)\sum_{m=1}^{M}\sin\left[\frac{2\pi}{T_i}(m-1)N\right]\Bigg\}, \end{aligned} \tag{4}$$

where T_i is the period. For $\mathrm{Er}_i = 0$ under any φ, $\sum_{m=1}^{M}\cos[(2\pi/T_i)(m-1)N]$ and $\sum_{m=1}^{M}\sin[(2\pi/T_i)(m-1)N]$ must both be zero. It can be proved that the solutions are of the following sorts:

$$N = (k/M)T_i \quad \text{and} \quad \mathrm{mod}(k, M) \neq 0, \tag{5}$$

where k is an integer. A PAM survey associated with M is called M phase. Some successful PAM surveys actually followed this principle. For example, in regions

TABLE 1. Relative error [Er_i in (4)] of each tidal constituent in different PAM surveys. Those that have been adopted for surveys in previous studies are marked by an asterisk. The PAM survey used in this study is marked by a double asterisk.

	S_2	M_2	N_2	K_2	K_1	O_1	P_1	Q_1	M_4	MS_4
*$M = 2$, $N = (1/2)T_{M_2}$	0.06	0	0.03	0.06	0.69	0.73	0.69	0.75	1	1
$M = 2$, $N = (2/3)T_{M_2}$	0.16	0	0.09	0.18	0.77	0.65	0.76	0.57	1	0.99
*$M = 2$, $N = (7/2)T_{M_2}$	0.38	0	0.21	0.40	0.84	0.55	0.82	0.36	1	0.93
$M = 3$, $N = (1/3)T_{M_2}$	0.04	0	0.02	0.04	0.64	0.69	0.65	0.71	0	0.04
*$M = 3$, $N = (2/3)T_{M_2}$	0.09	0	0.04	0.10	0.04	0.05	0.04	0.10	0	0.08
**M = 3, $N = (4/3)T_{M_2}$	0.15	0	0.09	0.16	0.10	0.09	0.08	0.16	0	0.18
*$M = 4$, $N = (2/4)T_{M_2}$	0.05	0	0.03	0.06	0.04	0.04	0.03	0.09	1	1
$M = 5$, $N = (1/5)T_{M_2}$	0.04	0	0.02	0.04	0.62	0.67	0.63	0.69	0	0.02
*$M = 5$, $N = (2/5)T_{M_2}$	0.05	0	0.03	0.05	0.04	0.04	0.03	0.09	0	0.08
$M = 5$, $N = (6/5)T_{M_2}$	0.18	0	0.13	0.19	0.08	0.07	0.06	0.13	0	0.12

controlled by one tidal constituent, say M_2, PAM surveys were conducted with $M = 2$ and $N = (1/2)T_{M_2}$ or $N = (7/2)T_{M_2}$ (Liu et al. 2000; Chang et al. 2008); $M = 3$ and $N = 8\,\mathrm{h}\,[\approx(2/3)T_{M_2}]$ (Chang et al. 2008); $M = 4$ and $N = 6.21\,\mathrm{h}\,[=(2/4)T_{M_2}]$ (Katoh et al. 1996, 2000); and $M = 5$ and $N = 5\,\mathrm{h}\,[\approx(2/5)T_{M_2}]$ (Chang et al. 2008).

Theoretically, an M_2-based PAM survey can safely eliminate the M_2 tidal constituent. However, it may be insufficient for other constituents such as diurnal or shallow-water tides. Even for the semidiurnal tides, S_2 for example, each has a period that is not exactly the same as M_2. Hence, it is necessary to estimate the error range induced by the M_2-based PAM survey. From (4), Er_i varies only with φ under particular values of M and N. Hence, the upper limits of relative errors Er_i can be numerically calculated by enumerating φ. Table 1 lists the error estimations for the major tidal constituents. It should be noted that the phase lags of different tidal constituents are actually correlated, so Er_i values cannot reach their upper limits at the same time. Hence, Table 1 only shows how the PAM survey works on the individual tidal constituents. A weighted mean of Er_i values based on their amplitudes could overestimate the total error.

From Table 1, it can be seen that all PAM surveys can completely remove the M_2 component and can largely remove the other semidiurnal constituents. Also, we can see that the following PAM surveys can largely remove the diurnal constituents: $M = 3$ and $N = (2/3)T_{M_2}$, $M = 3$ and $N = (4/3)T_{M_2}$, $M = 4$ and $N = (2/4)T_{M_2}$, $M = 5$ and $N = (2/5)T_{M_2}$, or $M = 5$ and $N = (6/5)T_{M_2}$. More generally, k in (5) should be an even number. This is because the periods of diurnal tides, for example K_1, are close to $2T_{M_2}$. Hence, $N = (k/M)T_{M_2} \approx (0.5k/M)T_{K_1}$, which also satisfies (5) if k is an even number. As constrained by $\mathrm{mod}(k, M) \neq 0$, M must be greater than 2. Similarly, to remove the shallow-water tidal currents with periods of $\sim 0.5T_{M_2}$, $\mathrm{mod}(2k, M)$ must not be zero according to (5). It should be noted that—although in this paper we only discuss the PAM surveys based on M_2—from (5), it is easy to design other kinds of PAM survey where the diurnal tide is dominant.

In practice, to determine the volume transport along one section, each site on the section should be repeated M times with exactly the same interval of N. For a one-ship survey, as conducted in this study, the ship needs to take measure at all the sites and come back to the first site in the interval of N, then repeat the survey at the exact same rhythm, so as to make all the sites to be measured for M rounds with the same interval of N. Hence, N is limited by the section length, ship speed, and sampling efficiency. When the survey region is large, such as the MZCC, N cannot be too small, but it also cannot be too large, as Er_i increases with N (Table 1). Also, M should be as small as possible to reduce the survey burden, which is the original purpose of a PAM survey. Taking all these requirements into consideration, we selected $M = 3$, $N = (4/3)T_{M_2} \approx 16.56\,\mathrm{h}$ to measure the MZCC. Theoretically, this can effectively remove the semidiurnal, diurnal, and shallow-water tides, and the survey interval is suitable for a large-scale, one-ship survey. Because the PAM survey only sampled for three times, it may be insufficient to remove the other high-frequency oscillations induced by, for instance, the synoptic wind variations. Fortunately, the wind during the survey was generally stable (discussed in section 2c).

b. The survey

Following the three-phase PAM principle, we designed a survey along a triangle-shaped section off the Min–Zhe Coast (Fig. 1, sites 1–15). The survey location was selected where the MZCC is free from disturbance of the Zhoushan Islands. Sites 1–8 crossed the slope with water depths ranging from 12.68 m at site 1 to 61.5 m at site 8, with a spacing of ~9.9 km. Sites 8–12 and sites 12–1 had a spacing of ~10 and ~20 km, respectively. The total distance for one complete survey round was ~190 km. Restricted by the ship speed, the sampling at

TABLE 2. PAM survey plan (scheduled PAM time in UTC +0800) and the actual measuring time (survey time). ADCP data length is the period of the useful ADCP data at each site, which is centered at survey time. At each site, we also measured the salinity and temperature profiles using a CTD, and took water samples for other studies. Sites 9–15 are not listed in the table, because they were abandoned on the third PAM round because of bad weather.

Site	Scheduled PAM time	Survey time	ADCP data length (min)
	First PAM round		
1	0900 9 Feb	0900 9 Feb	6
2	0954 9 Feb	0957 9 Feb	7.5
3	1048 9 Feb	1047 9 Feb	8.4
4	1142 9 Feb	1140 9 Feb	7.5
5	1236 9 Feb	1234 9 Feb	8.5
6	1330 9 Feb	1328 9 Feb	12
7	1425 9 Feb	1425 9 Feb	10
8	1519 9 Feb	1518 9 Feb	9
	Second PAM round		
1	0133 10 Feb	0132 10 Feb	9.9
2	0227 10 Feb	0227 10 Feb	12
3	0321 10 Feb	0321 10 Feb	10.2
4	0416 10 Feb	0415 10 Feb	10.5
5	0510 10 Feb	0509 10 Feb	10
6	0604 10 Feb	0601 10 Feb	13
7	0658 10 Feb	0656 10 Feb	11.5
8	0752 10 Feb	0752 10 Feb	9.6
	Third PAM round		
1	1807 10 Feb	1803 10 Feb	8.3
2	1901 10 Feb	1859 10 Feb	10.6
3	1955 10 Feb	1955 10 Feb	9.8
4	2049 10 Feb	2049 10 Feb	5.4
5	2143 10 Feb	2143 10 Feb	6.3
6	2238 10 Feb	2235 10 Feb	7.4
7	2332 10 Feb	2333 10 Feb	3.7
8	0026 11 Feb	0029 11 Feb	6.1

each site must be finished in a short time (~15 min) to complete sites 1–15 and go back to site 1 in $N = (4/3)T_{M_2} \approx 16.56$ h. To successfully remove the tidal signals by the PAM survey, the key is to carefully design the survey and to operate very precisely in the field. The scheduled PAM survey and its implementation status in the field are summarized in Table 2. Before the survey, we verified this plan by mimicking the PAM survey using numerical model (Wu et al. 2011), and the residual currents from the "PAM survey" were almost identical to the low-pass-filtered data. In the field, we were successful in following the schedule precisely until after sampling at site 8 on the third round. At that time, the weather conditions worsened, and the survey was terminated. Nevertheless, we obtained complete current data at sites 1–8, which was sufficient for quantifying the MZCC.

A 300-kHz downward-looking ADCP (Teledyne RD Instrument) equipped with an electric gyro and a differential global positioning system (DGPS) was mounted at the bottom of the ship to measure the current profile with a vertical resolution of 1 m and a sampling interval of 4 s. The ADCP transducer was placed 2.45 m below the sea surface, and the upper blank layer was 1.8 m. The lower blank layer varied from 2 to 4 m, increasing with the water depth. A Seabird Electronics 25 (SBE25) CTD was slowly lowered to profile the temperature and salinity with a sampling interval of 0.5 s. At each site, the useful ADCP measurement lasted for a period of ~4–10 min, with the central time deviating at most 4 min from the scheduled PAM time (Table 2). After averaging in this period, the high-frequency oscillations of velocity caused by the waves and the ship's pitch and roll can be filtered out. The ADCP worked well with a percent good (100% is excellent) greater than 95% for data quality at all sites. Although measurements were also conducted at other sites shown in Fig. 1, this study focused on sites 1–8. During the entire survey (from 5 to 14 February), an SBE37 CTD was used to measure the sea surface salinity with a sampling interval of 6 s in water pumped by the ship's cooling system.

c. *Hydrological and weather conditions*

The mean Changjiang runoff (observed by the *Changjiang Water Resource Commission* at Datong Hydrographic Station, which is ~630 km away from the river mouth) in the 20 days prior to the PAM survey was $(15.7 \pm 1.1) \times 10^3\,m^3\,s^{-1}$ (Fig. 2a). For reference, the Changjiang discharge was $(15.9 \pm 3.4) \times 10^3\,m^3\,s^{-1}$ from October 2011 to February 2012; then it suddenly rose to $(25.8 \pm 5.1) \times 10^3\,m^3\,s^{-1}$ in March. Climatologically, since the closure of Three Gorges Dam in 2003, the Changjiang discharge from October to March has been $(16.8 \pm 5.9) \times 10^3\,m^3\,s^{-1}$. Hence, the Changjiang runoff during the MZCC-developed seasons is relatively stable, and the discharge during the PAM survey, $15.7 \times 10^3\,m^3\,s^{-1}$, was typical. There are also several small rivers along the Zhejiang Coast, with the major one being the Qiantang River discharging into the Hangzhou Bay. However, their runoffs are far smaller than that from Changjiang. For example, the runoff of Qiantang River was $578\,m^3\,s^{-1}$ in January 2012 (observed by the *Zhejiang Provincial Hydrology Bureau*), ~3.7% of the Changjiang runoff. Moreover, its mouth is far from the MZCC.

Tidal elevation (Fig. 2b) was recorded at Shipu, which is close to the survey area. The PAM survey was during the spring tide with a tidal range of ~5.0 m. Tidal mixing can amplify the MZCC both for the volume transport

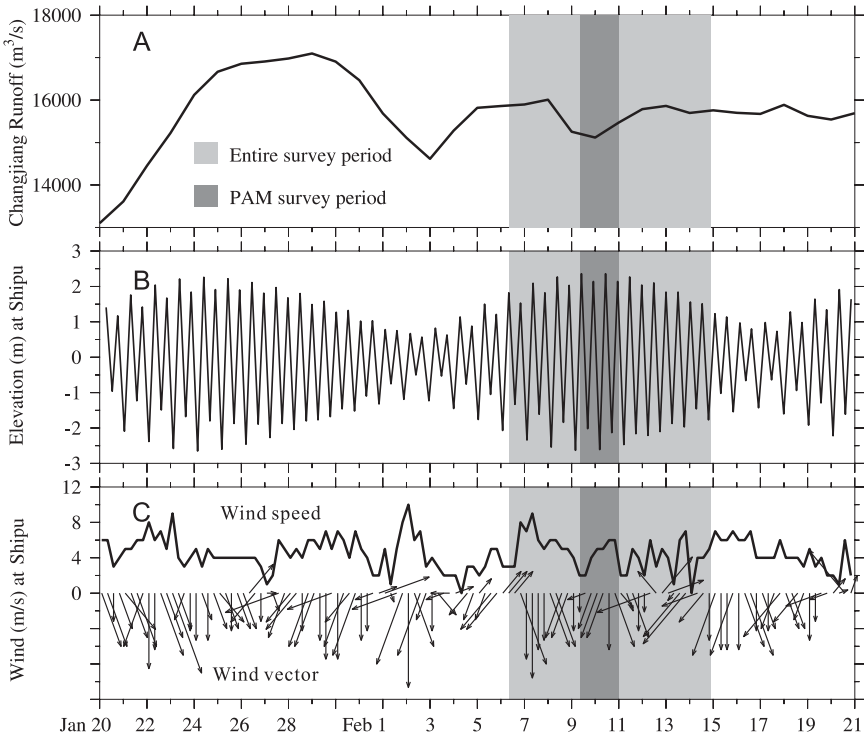

FIG. 2. Hydrological and weather conditions. (a) Changjiang runoff, (b) tidal elevation measured at Shipu (for location see Fig. 1), and (c) wind vector and speed measured at Shipu.

and for the freshwater transport, as has been demonstrated recently by Li and Rong (2012). However, the variation of transport during a spring–neap cycle seems to be an order of magnitude smaller than the transport itself (see their Fig. 7).

The 6-hourly record (Fig. 2c) at Shipu shows that the wind, with a maximum speed of $6\,m\,s^{-1}$, was largely stable and mainly northerly during the PAM survey. According to the National Centers for Environmental Prediction (NCEP)/Quick Scatterometer (QuikSCAT) dataset, the monthly wind from October to March around the survey region is relatively stable (-0.55 ± 0.8 and $-5.74 \pm 0.89\,m\,s^{-1}$ in the zonal and meridional directions, respectively). Hence, the weather conditions during this PAM survey were typical for the winter season.

3. Results

a. Current, salinity, and temperature

The sea surface salinity obtained with the SBE37-CTD is plotted in Fig. 1, from which one can see buoyant water along the isobaths with low salinity. Generally, the diluted water was confined landward at depths shallower than ~40 m and with salinity ranging from 28–29 to 34 outside the front. The location of the observed salinity front was similar to its climatological position (Fig. 1), indicating that the buoyant coastal current we measured was typical. The offshore extents of diluted water were similar on all sections (i.e., ECD1–ECD4, 1–8, and ECB1–ECB6), suggesting that the MZCC measured along sites 1–8 was representative.

The direct current measurements in each PAM round are shown in Fig. 3. As the three-phase-averaging survey measured the current with an interval of $(4/3)T_{M_2}$ and the tidal current is rotating off the Min–Zhe Coast, it can be expected that the three measured current vectors roughly trisected the tidal ellipse. This was particularly evident at site 1, where the tidal motion is dominant. However, as modulated by the MZCC, currents at sites 2–4 showed notable southward-flowing tendencies.

Averaging the currents from three PAM rounds showed a clear signal of the MZCC (Fig. 1, residual currents at 4.25 m below the sea surface). The residual currents were southwestward at sites 2, 3, and 4, with velocities of 29.1, 47.2, and $40.0\,cm\,s^{-1}$, respectively, close to that measured by Zhu et al. (2004) ($50\,cm\,s^{-1}$). At the deeper offshore sites, that is, sites 5–8, the residual currents were mainly northward, a possible indication of the TWC, which can reach this region in winter (Zhu et al. 2004).

Residual currents were further decomposed into the two components across and along the section (i.e., sites

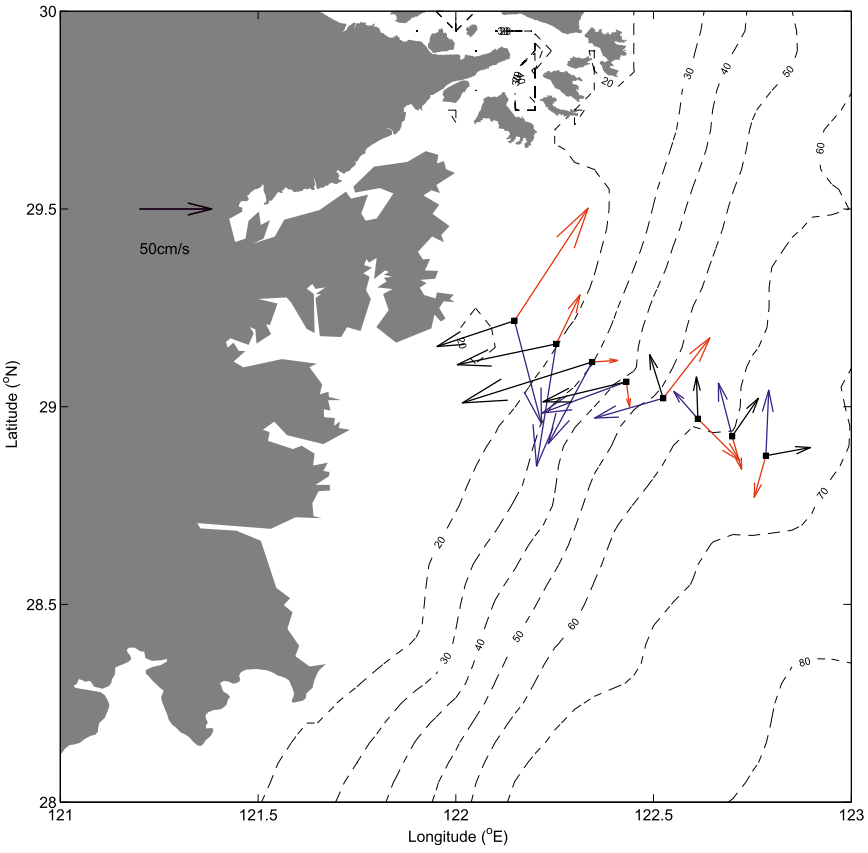

FIG. 3. Directly measured currents (4.25 m below the sea surface) during each PAM round. Red: the first round; Blue: the second round; Black: the third round.

1–8), as shown in Fig. 4. These two components were used to represent the alongshore and cross-shelf components, respectively. Thick dashed lines depict the upper and lower ADCP blank layers. The observed residual currents had a good linear characteristic in the vertical, with $r^2 > 0.99$ at sites 2–4, and $r^2 > 0.96$ at the other sites, under the confidence level of 98%. Hence, the velocities in the blank layers were linearly extrapolated to further calculate the transports. Because the salinity and temperature varied along with the tide, the three-phase PAM method was also applied to remove their tidal oscillations, as shown in Fig. 5. From these sectional profiles, it is clear that the MZCC was confined to the slope region inside the 40-m isobath. The lower salinity (Fig. 5a) suggested that the MZCC was transporting the Changjiang-diluted water. The temperature was also lower than it was in the offshore regions, possibly because the Changjiang water was sufficiently cooled on the land in winter, or because there was intensified heat loss in the shallow coastal waters. From the geometry of the salinity and temperature profiles, it can be seen that the Changjiang-diluted water extended along the Min–Zhe Coast as a bottom-trapped plume, because the isohalines intersected the sea bed (Yankovsky and Chapman 1997). The warmer northward currents off of the 40-m isobath were generally uniform in the vertical with a magnitude around $10\,\mathrm{cm\,s^{-1}}$. However, in the lower layers of site 5, they were intensified, with speeds greater than $15\,\mathrm{cm\,s^{-1}}$. This was probably influenced by the upshelfward near-bottom countercurrent for buoyant coastal currents, which halts the offshore bottom buoyancy transport and drives the plume to a steady status (Chapman and Lentz 1994). The plume-front depth was a little deeper than the theoretical prediction based on the formula of Yankovsky and Chapman (1997), which only gives a depth of ~31 m. This was probably due to the downwelling-favorable wind and the constraint of the Taiwan Warm Current, both of which push the isohalines to the coast at the surface and to the offshore at the bottom.

For the cross-shelf direction, the onshore tendency can be detected in almost the entire water column at sites 2–5 (Fig. 4b), unlike the expectation for a bottom-trapped plume. Chapman and Lentz (1994) found that for a bottom-trapped plume, the cross-shelf flow converges at the foot of the front, which was not seen in Fig. 4b. However, it can still be seen that the near-bottom

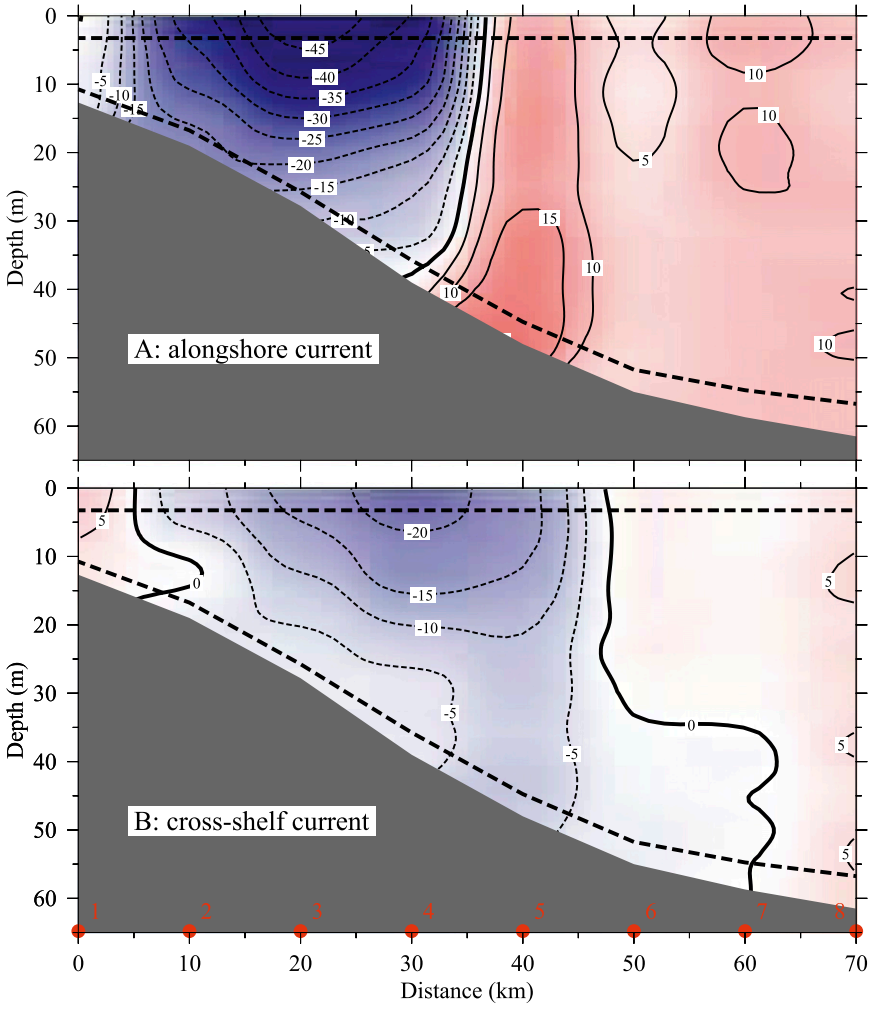

FIG. 4. Sectional profiles of the residual currents ($cm\,s^{-1}$) measured along sites 1–8. (a) Alongshore current (northward positive) and (b) cross-shelf current (eastward positive). Red dots and numbers signify the sites. Thick dashed lines indicate the upper and lower blank layers.

onshore velocity was smaller at sites 2–4 than at site 5, which seemed to be a convergent point between sites 4 and 5. Because the Min–Zhe Coast is not straight and because the way we decomposed the current into alongshore and cross-shelf components was simply based on the transection of sites 1–8, Fig. 4b might not be the exact cross-shelf component. It can thus be expected that, by rotating to a certain angle, the near-bottom convergent cross-shelf flow will be more evident. However, as the main purpose of this study was to determine the alongshore transports, this was not pursued.

b. *Volume transport*

The volume transport of the MZCC was calculated based on the observed residual current profiles: $T = \sum_{v<0}(vdzdx)$, where v is the velocity component normal to the section, dz is the vertical interval, and dx is the horizontal interval of 9.9 km. The resulting value was 0.215 Sv—to the best of our knowledge, the first measured value of the volume transport of the MZCC. The volume transport directly calculated from the ADCP bins was 0.163 Sv. Those estimated from the upper and lower blank layers were 0.044 and 0.008 Sv, respectively. The measured volume transport was 13.7 times the 20-day-mean Changjiang discharge prior to the PAM survey, or 12.6 times the peak discharge during that period. Conservatively speaking, it was $O(10)$ times the Changjiang discharge, considering that the exact response time of the MZCC to the Changjiang runoff is unclear and that there might be other uncertainties in the observations.

c. *Freshwater transport*

The freshwater transport of the MZCC can be calculated by $Pf = \int_A vF\,dA$, where A is the cross-sectional

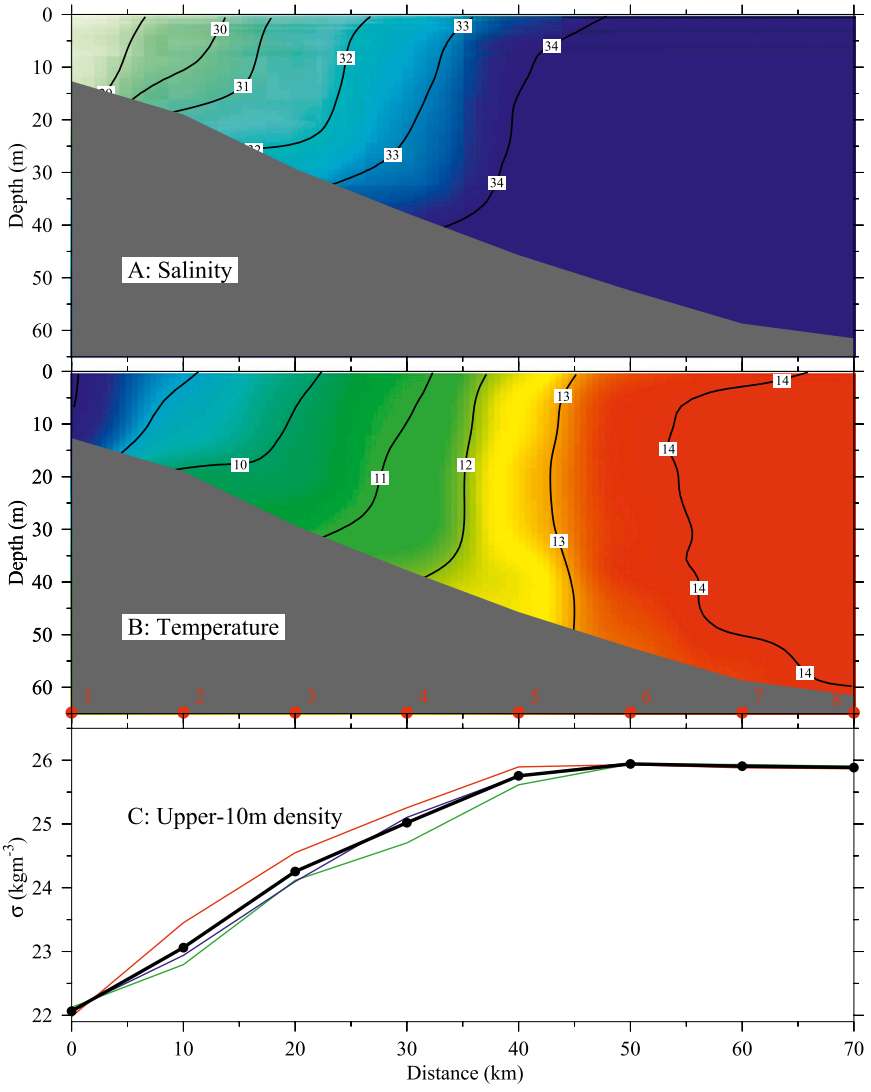

FIG. 5. Sectional profiles of (a) the averaged salinity and (b) the temperature along sites 1–8. (c) The upper-10-m density anomaly observed in each PAM round (colored lines) and their mean value (thick black line). Red dots and numbers signify the sites.

area of the MZCC, $F = (s_o - s)/s_o$ is the freshwater fraction, s_o is the reference salinity, and s is the observed salinity. From Fig. 5, the boundary of the buoyant water can be represented by the 34 isohaline; hence, we set s_o to this value. The resultant Pf was $15.2 \times 10^3\,m^3\,s^{-1}$, close to the mean Changjiang river discharge (i.e., Rf) during the prior 20 days ($15.7 \times 10^3\,m^3\,s^{-1}$), or even to the peak runoff during that period ($17.1 \times 10^3\,m^3\,s^{-1}$). Hence, Pf/Rf is ~97%, with a lower limit of 89% if compared to the peak runoff. The estimation of this ratio might contain some uncertainties, because the exact response time of the MZCC to the Changjiang runoff is unclear, and the choice of 20 days is debatable. To get a more accurate dependence of MZCC on the Changjiang runoff, long-term observations or numerical model simulations would be required in further studies. Moreover, the Qiantang River could also contribute to the freshwater transport of the MZCC, but its contribution should be small as indicated by its small runoff. Nevertheless, it is reasonable to say that over 90% of the Changjiang runoff was transported by the MZCC. Different selections of s_o between 34 and 34.33 (highest salinity observed) only resulted in slight differences.

4. Discussion

a. *Freshwater transport*

The observed freshwater transport by the MZCC was very close to that from the Changjiang, with $Pf/Rf > 90\%$.

Theoretically, freshwater transport by a buoyant coastal current often differs from the river discharge because of the possible development of a recirculating plume bulge or cross-frontal mixing. This deviation becomes evident when the discharge Rossby number $R_o = U/Bf$ is large, where U is the river inflow velocity, f is the Coriolis parameter, and B is the mouth width. However, it has been found that, under downshelfward background currents, the value of Pf approaches that of Rf after a certain period (Fong and Geyer 2002). A recent study further indicated that tidal mixing can stabilize the plume bulge and favor increasing the freshwater transport by the buoyant coastal current (Li and Rong 2012).

Because of the wide river mouth of the Changjiang and the relative lower river discharge in winter, the value of R_o was small during the period we studied. It was estimated to be only ~0.05, which is insufficient to develop a significant plume bulge. Actually, none of the past observations in winter has found the plume bulge, and the plume extends along the coast (see Fig. 1 for the climatological pattern). In a model study, Li and Rong (2012) found that the ratio between the freshwater transport by the MZCC and the Changjiang runoff, that is, Pf/Rf, is as large as ~80%, even in the absence of the downwelling-favorable wind. In February, as a matter of fact, the northerly winter monsoon had already lasted over three months, which is long enough to establish a downshelf wind-driven background current to further approach Pf to Rf (Fong and Geyer 2002). Hence, it can be expected that for the MZCC, Pf/Rf should be close to 1.

b. Vertical current shear

Figure 5 shows a pattern of a bottom-trapped plume; hence the current profile should follow the thermal–wind relationship (Yankovsky and Chapman 1997). Because the cross-shelf density gradient can be largely treated as approximately constant with depth for a bottom-trapped plume, we used the upper-10-m density anomaly σ (by subtracting 1000 kg m^{-3}) as a representation to calculate the horizontal density gradient. The σ values of the three PAM rounds are distinguished by the colored lines, and their mean is shown as a thick black line (Fig. 5c). It can be seen that the mean density anomaly varied linearly from site 1 to 5, and thereafter it became almost constant. The mean density gradient ρ_x from site 1 to 5 was 0.9224×10^{-4} kg m^{-3} m^{-1}. Under the thermal–wind balance, the vertical current shear $v_z = -g\rho_x/(\rho_o f)$, where z is the height above the seabed, g is the gravity, ρ_o is the ocean density, and the Coriolis parameter f is 0.707×10^{-4} s^{-1} at latitude of 29°N. The density ρ_o was calculated for a salinity of 34 and a temperature of 14°C, resulting in a value of 1025.6 kg m^{-3}. Hence, $v_z \approx 1.25$ cm s^{-1} m^{-1}, while the measured residual velocity showed linear shears of 0.86, 1.49, and 1.14 cm s^{-1} m^{-1} at sites 2, 3, and 4, respectively. The relatively large discrepancy at site 2 could have resulted from disturbance by bottom friction where the depth was relatively shallow and the tide was strong. The good agreement at sites 3 and 4 indicates that the vertical current shears were determined mainly by the buoyancy. Bottom velocity was close to zero at site 4, where the base of the front was located.

c. Volume transport

Under the combined effects of the buoyancy and the downwelling-favorable winds, the total volume transport can be decomposed into $T \approx T_\rho + T_W$, where T_ρ and T_W are transports driven by buoyancy and wind, respectively. This linear relationship was justified by Münchow and Garvine (1993) and Lentz and Largier (2006). For the buoyant part, Yankovsky and Chapman (1997) suggested $T_\rho = g'h^2/2f$ for a bottom-trapped plume with a sharp front, where g' is the reduced gravity inside the front, and h is the maximum plume depth. Pimenta et al. (2011) extended this relationship to buoyant coastal currents with various frontal widths. In particular, for the case of wide front, the density-driven transport is $T_\rho = g'h^2/6f$ (Avicola and Huq 2002; Pimenta et al. 2011). As can be seen in Fig. 5, the density inside the MZCC varied gradually from the coast to the offshore limit, which can be considered as a wide front. Thus, T_ρ was estimated to be 0.128 Sv, similar to the estimation by Li and Rong (2012) from a simulation, but it can only explain ~60% of the total volume transport.

The remaining volume transport most likely came from the downwelling-favorable wind. Downwelling-favorable wind drives a downshelf-flowing coastal current either by direct drag stress or by setting up a cross-shelf barotropic gradient, both of which favor the intensification of the MZCC. Moreover, the wind can modulate the buoyancy structure of the MZCC, thus impacting the buoyant part of the volume transport. Because the wind is variable in both time and space and because the coastal current needs some time to fully respond to the wind, an in-depth investigation of wind effects on the MZCC would require further long-term observations or numerical simulations.

5. Summary

Based on a phase-averaging cruise survey, we have successfully measured the subtidal characteristics of the Min–Zhe Coastal Current (MZCC). The MZCC was found to flow southward along the slope region off the Min–Zhe Coast, with a maximum surface speed of

$\sim 50\,\mathrm{cm\,s^{-1}}$. For the first time, we measured its volume transport, which was found to be 0.215 Sv, $O(10)$ times that of the Changjiang River, transporting over 90% of the freshwater from Changjiang. Buoyancy and wind are two major forcings to drive the MZCC, and the former contributed about 0.128 Sv of the observed volume transport.

Acknowledgments. The authors express sincere thanks to editor Parker MacCready and two anonymous reviewers for their constructive comments on improving the manuscript. We also wish to express our sincere appreciation to Mr. Hongguang Zhu, Captain Guohua Zhou, and the entire crew of the R/V *Runjiang I* for their highly skillful navigation and cooperation. This study was jointly supported by the Funds for Creative Research Groups of China (Grant 41021064) and National Basic Research Program of China (Grant 2011CB409801).

REFERENCES

Avicola, G., and H. Huq, 2002: Scaling analysis for the interaction between a buoyant coastal current and the continental shelf: Experiments and observations. *J. Phys. Oceanogr.,* **32,** 3233–3248.

Beardsley, R. C., R. Limeburner, H. Yu, and G. A. Cannon, 1985: Discharge of the Changjiang (Yangtze River) into the East China Sea. *Cont. Shelf Res.,* **4,** 57–76.

Candela, J., R. C. Beardsley, and R. Limeburner, 1992: Separation of tidal and subtidal currents in ship-mounted acoustic Doppler current profilers' observations. *J. Geophys. Res.,* **97** (C1), 769–788.

Chang, Y. C., R. S. Tseng, and C. T. Liu, 2008: Evaluation of tidal removal method using phase average technique from ADCP surveys along the Peng-Hu Channel in the Taiwan Strait. *Terr. Atmos. Oceanic Sci.,* **19,** 433–443.

Chapman, D. C., and S. J. Lentz, 1994: Trapping of a coastal density front by the bottom boundary layer. *J. Phys. Oceanogr.,* **24,** 1464–1479.

Chen, C. T. A., 2008: Distributions of nutrients in the East China Sea and the South China Sea connection. *J. Oceanogr.,* **64,** 737–751.

Dai, A., and K. Trenberth, 2002: Estimates of freshwater discharge from continents: Latitudinal and seasonal variations. *J. Hydrometeor.,* **3,** 660–687.

Deng, B., J. Zhang, and Y. Wu, 2006: Recent sediment accumulation and carbon burial in the East China Sea. *Global Biogeochem. Cycles,* **20,** GB3014, doi:10.1029/2005GB002559.

Editorial Board for Marine Atlas, 1992: *Marine Atlas of Bohai Sea, Yellow Sea and East China Sea (Hydrology).* China Ocean Press, 524 pp.

Fong, D. A., and W. R. Geyer, 2002: The alongshore transport of freshwater in a surface-trapped river plume. *J. Phys. Oceanogr.,* **32,** 957–972.

Garvine, R. W., 1995: A dynamical system for classifying buoyant coastal discharges. *Cont. Shelf Res.,* **15,** 1585–1596.

Geyer, W. R., R. P. Signell, D. A. Fong, J. Wang, D. M. Anderson, and B. A. Keafer, 2004: The freshwater transport and dynamics of the western Maine coastal current. *Cont. Shelf Res.,* **24,** 1339–1357.

Guan, B., 1978: Characteristics of the East China Sea current system (in Chinese). *Essays on the East China Sea Shelf,* Institute of Oceanology, 126–133.

Hickey, B., S. Geier, N. Kachel, and A. MacFadyen, 2005: A bi-directional river plume: The Columbia in summer. *Cont. Shelf Res.,* **25,** 1631–1656.

Howden, S. D., and R. Murtugudde, 2001: Effects of river inputs into the Bay of Bengal. *J. Geophys. Res.,* **106** (C9), 19 825–19 843.

Jan, S., and S. Y. Chao, 2003: Seasonal variation of volume transport in the major inflow region of the Taiwan Strait: The Penghu Channel. *Deep-Sea Res. II,* **50,** 1117–1126.

Katoh, O., K. Teshima, O. Abe, H. Fujita, K. Miyaji, K. Morinaga, and N. Nakagawa, 1996: Process of Tsushima Current formation revealed by ADCP measurements in summer. *J. Oceanogr.,* **52,** 491–507.

——, K. Mornaga, and N. Nakagawa, 2000: Current distributions in the southern East China Sea in summer. *J. Geophys. Res.,* **105** (C4), 8565–8573.

Lentz, S. J., and J. Largier, 2006: The influence of wind forcing on the Chesapeake Bay buoyant coastal current. *J. Phys. Oceanogr.,* **36,** 1305–1316.

Li, M., and Z. Rong, 2012: Effects of tides on freshwater and volume transport in the Changjiang River plume. *J. Geophys. Res.,* **117,** C06027, doi:10.1029/2011JC007716.

Lin, S. W., I. J. Hsieh, K. M. Huang, and C. H. Wang, 2002: Influence of the Yangtze River and grain size on the spatial variations of heavy metals and organic carbon in the East China Sea continental shelf sediments. *Chem. Geol.,* **182,** 377–394.

Liu, J. P., A. C. Li, K. H. Xu, D. M. Velozzi, Z. S. Yang, J. D. Milliman, and D. J. DeMaster, 2006: Sedimentary features of the Yangtze River-induced along-shelf clinoform deposit in the East China Sea. *Cont. Shelf Res.,* **26,** 2141–2156.

Liu, K. K., T. Y. Tang, G. C. Gong, L. Y. Chen, and F. K. Shiah, 2000: Cross-shelf and along-shelf nutrient fluxes derived from flow fields and chemical hydrography observed in the southern East China Sea off northern Taiwan. *Cont. Shelf Res.,* **20,** 493–523.

Liu, S. M., and J. Zhang, 2000: Chemical oceanography of nutrient elements in the Bohai Sea, Yellow Sea, and East China Sea. *Mar. Sci. Bull.,* **2,** 76–85.

Lü, X., F. Qiao, C. Xia, J. Zhu, and Y. Yuan, 2006: Upwelling off the Yangtze River estuary in summer. *J. Geophys. Res.,* **111,** C11S08, doi:10.1029/2005JC003250.

Milliman, J. D., H. T. Shen, Z. S. Yang, and R. H. Meade, 1985: Transport and deposition of river sediment in the Changjiang estuary and adjacent continental shelf. *Cont. Shelf Res.,* **4,** 37–45.

Münchow, A., 2000: Detiding three-dimensional velocity survey data in coastal waters. *J. Atmos. Oceanic Technol.,* **17,** 736–748.

——, and R. W. Garvine, 1993: Buoyancy and wind forcings of a coastal current. *J. Mar. Res.,* **51,** 293–322.

Niino, H., and K. O. Emery, 1961: Sediments of shallow portions of East China Sea and South China Sea. *Geol. Soc. Amer. Bull.,* **72,** 731–762.

Pimenta, F. M., A. D. Kirwan Jr., and P. Huq, 2011: On the transport of buoyant coastal plumes. *J. Phys. Oceanogr.,* **41,** 620–640.

Qiao, F., Y. Yang, X. Lü, C. Xia, X. Chen, B. Wang, and Y. Yuan, 2006: Coastal upwelling in the East China Sea in winter. *J. Geophys. Res.,* **111,** C11S06, doi:10.1029/2005JC003264.

Rossby, T., and C. N. Flagg, 2012: Direct measurement of volume flux in the Faroe–Shetland Channel and over the Iceland–Faroe Ridge. *Geophys. Res. Lett.,* **39,** L07602, doi:10.1029/2012GL051269.

Shen, H., Z. Mao, and J. Zhu, 2003: *Saltwater Intrusion in the Changjiang Estuary.* China Ocean Press, 175 pp.

Simpson, J. H., 1997: Physical processes in the ROFI regime. *J. Mar. Syst.,* **12,** 3–15.

——, E. G. Mitchelson-Jacob, and A. E. Hill, 1990: Flow structure in a channel from acoustic Doppler current profiler. *Cont. Shelf Res.,* **10,** 589–603.

Su, J., and Y. Yuan, Eds., 2005: *Oceanography of China Seas*. China Ocean Press, 367 pp.

Whitney, M. M., and R. W. Garvine, 2005: Wind influence on a coastal buoyant outflow. *J. Geophys. Res.,* **110,** C03014, doi:10.1029/2003JC002261.

Wu, H., J. Zhu, J. Shen, and H. Wang, 2011: Tidal modulation on the Changjiang River plume in summer. *J. Geophys. Res.,* **116,** C08017, doi:10.1029/2011JC007209.

Yankovsky, A. E., and D. C. Chapman, 1997: A simple theory for the fate of buoyant coastal discharges. *J. Phys. Oceanogr.,* **27,** 1386–1401.

Zeng, D. Y., X. B. Ni, and D. J. Huang, 2012: 2012: Temporal and spatial variability of the ZheMin Coastal Current and the Taiwan Warm Current in winter in the southern Zhejiang coastal area (in Chinese). *Sci. Sin. Terrae,* **42,** 1123–1134.

Zhang, H., P. Du, and X. Zheng, 2011: Characteristics analysis of residual current of Zhejiang-Fujian water (in Chinese). *Mar. Sci. Bull.,* **30,** 152–158.

Zhu, J., C. Chen, P. Ding, C. Li, and H. Lin, 2004: Does the Taiwan warm current exist in winter? *Geophys. Res. Lett.,* **31,** L12302, doi:10.1029/2004GL019997.